Kirchhoff prestack depth scalar migration in a simple triclinic velocity model for three-component P, S and converted waves

Václav Bucha
Department of Geophysics, Faculty of Mathematics and Physics, Charles University, Ke Karlovu 3, 121 16 Praha 2, Czech Republic, bucha@seis.karlov.mff.cuni.cz

Summary

We use 3-D ray-based Kirchhoff prestack depth scalar migration to calculate migrated sections in a simple homogeneous triclinic velocity model. The ray-theory three-component recorded wave field corresponding to reflected P, S1, S2 and converted waves is generated in the velocity model composed of two homogeneous layers separated by a curved interface. The anisotropy of the upper layer is triclinic and the bottom layer is isotropic. We apply 3-D Kirchhoff prestack depth scalar migration to single-layer velocity model with the same triclinic anisotropy as in the upper layer of the velocity model used to calculate the recorded wave field. We show and discuss the results of the migration for individual components of individual types of waves.

Keywords

3-D Kirchhoff prestack depth scalar migration, anisotropic velocity model, triclinic anisotropy, elastic waves, three-component seismograms

1. Introduction

There are two basic families of prestack depth migrations of multicomponent seismic data: scalar migration and elastic migration (Hou & Marfurt, 2002). From another point of view, migration of multicomponent data has been attempted using either ray-based or wave-based solutions (Wang & McMechan, 2016). Different migration approaches have of course some advantages, disadvantages and limitations (e.g., Gray et al., 2001).

The acoustic (scalar) Kirchhoff migration method is very popular in the industrial world because of its high computational efficiency and flexible imaging while the elastic Kirchhoff migration method is developing slowly (Qizhen & Bo, 2008).

Kuo & Dai (1984) and Qizhen & Bo (2008) presented prestack elastic Kirchhoff migration in 2-D isotropic elastic media for reflected PP and converted PS waves. Hokstad (2000) derived equations for elastic and viscoelastic Kirchhoff migration of multicomponent seismic data. However, the theory requires complete boundary conditions on the receiver side, i.e., measurement of both displacement and traction (pressure) that is rare in seismic experiments. Hokstad (2000) implemented the method for imaging of marine multicomponent seismic data in 2-D horizontally layered anisotropic velocity models for reflected PP, SS and converted PS waves.

In this paper we continue in 3-D ray-based Kirchhoff prestack depth scalar migration studies. While the previous studies were limited to vertical component of P waves, in this paper we use three-component ray-theory P, S1, S2 and converted waves.

Seismic Waves in Complex 3–D Structures, **28** (2018), 61–84 (ISSN 2336–3827, online at http://sw3d.cz)

The dimensions of the velocity model, shot-receiver configuration, methods for calculation of the recorded wave field and the migration are the same as in the previous papers by Bucha (e.g., 2012, 2013, 2017), where we studied the sensitivity of the migrated images to incorrect anisotropy, to incorrect gradients of elastic moduli or to incorrect rotation of the tensor of elastic moduli (stiffness tensor).

We generate three-component synthetic seismograms of reflected P, S1, S2 and converted waves (nine elementary waves) using the ray theory which is approximate. We apply the ANRAY software package (Gajewski & Pšenčík, 1990). We consider radial, transversal and vertical components. To compute the synthetic recorded wave field, we use simple anisotropic velocity model composed of two homogeneous layers separated by one curved interface that is non-inclined in the direction perpendicular to the source-receiver profiles. The anisotropy in the upper layer is triclinic and is thus not mirror symmetric. The complexity of the anisotropy is obvious from the generated and displayed ray-velocity surfaces of P, S1 and S2 waves. The bottom layer is isotropic.

We then migrate separately individual components of individual waves using 3-D ray-based Kirchhoff prestack depth scalar migration in the single-layer triclinic velocity model. The elastic moduli in the velocity model correspond to the upper layer of the velocity model in which the synthetic seismograms have been calculated. For migration we utilize MODEL, CRT, FORMS and DATA software packages (Červený, Klimeš & Pšenčík, 1988; Bulant, 1996; Bucha & Bulant, 2017). The packages used for calculation of the recorded wave field and for the migration are independent.

2. Anisotropic velocity model

The dimensions of the velocity model and the measurement configuration are derived from the 2-D Marmousi model and dataset (Versteeg & Grau, 1991). The horizontal dimensions of the velocity model are 0 km $\leq x_1 \leq$ 9.2 km, 0 km $\leq x_2 \leq$ 10 km and the depth is 0 km $\leq x_3 \leq$ 3 km. The velocity model is composed of two layers separated by one curved interface (see Figure 1). The curved interface is non-inclined in the direction of the x_2 axis which is perpendicular to the source-receiver profiles.

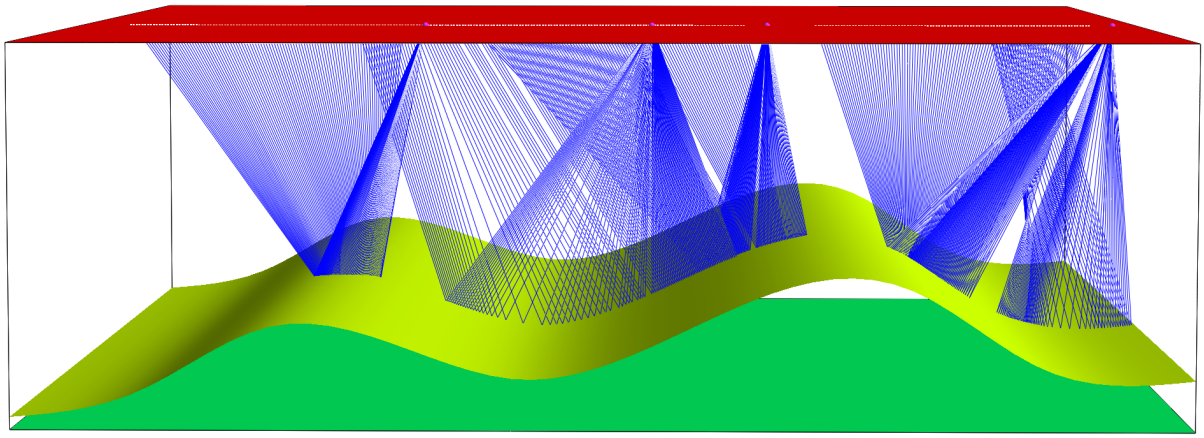

Figure 1. Velocity model with a curved interface and with triclinic anisotropy in the upper layer. The horizontal dimensions of the velocity model are 0 km $\leq x_1 \leq$ 9.2 km, 0 km $\leq x_2 \leq$ 10 km and the depth is 0 km $\leq x_3 \leq$ 3 km. The velocity model contains one curved interface which is non-inclined in the direction perpendicular to the source-receiver profiles. Two-point rays of the converted PS2 wave for one selected profile line (at horizontal coordinate $x_2 = 6$ km) and four shot-receiver configurations (from the left-hand side: shots 1, 80, 120 and 240 along the profile) are displayed.

The recorded wave field is computed in the velocity model composed of two homogeneous layers. The medium in the upper layer of the velocity model is triclinic. The bottom layer is isotropic.

The triclinic medium is represented by dry Vosges sandstone (Mensch & Rasolofosaon, 1997). Triclinic anisotropy is asymmetric. The matrix of density-reduced elastic moduli in km^2/s^2 reads

$$\begin{pmatrix} 10.3 & 0.9 & 1.3 & 1.4 & 1.1 & 0.8 \\ & 10.6 & 2.1 & 0.2 & -0.2 & -0.6 \\ & & 14.1 & 0.0 & -0.5 & -1.0 \\ & & & 5.1 & 0.0 & 0.2 \\ & & & & 6.0 & 0.0 \\ & & & & & 4.9 \end{pmatrix}. \tag{1}$$

The value of anisotropy strength defined as $2(P_{max} - P_{min})/(P_{max} + P_{min}) \times 100\%$ is 17 % , where P_{min} and P_{max} are minimum and maximum absolute norms of the slowness vector. The P-wave velocity in the isotropic bottom layer is $V_p = 3.6$ km/s and the S-wave velocity is $V_s = V_p/\sqrt{3}$.

We migrate in the single-layer velocity model (without the curved interface) with the same triclinic anisotropy given by matrix (1). The elastic moduli in the velocity model correspond to the upper layer of the velocity model in which the synthetic data have been calculated.

3. Shots and receivers

The measurement configuration is derived from the Marmousi model and dataset (Versteeg & Grau, 1991). The profile lines are parallel with the x_1 coordinate axis. Each profile line has the following configuration: The first shot is 3 km from the left-hand side of the velocity model, the last shot is 8.975 km from the left-hand side of the velocity model (see Figure 1), the distance between the shots is 0.025 km, and the depth of the shots is 0 km. The total number of shots along one profile line is 240. The number of receivers per shot is 96, the first receiver is located 2.575 km left of the shot location, the last receiver is 0.2 km left of the shot location, the distance between the receivers is 0.025 km, and the depth of the receivers is 0 km. This configuration simulates a simplified towed streamed acquisition geometry.

The 3-D measurement configuration consists of 81 parallel profile lines, see Figure 2. The interval between the parallel profile lines is 0.025 km.

4. Recorded wave field

The recorded wave field in the triclinic velocity model (with the curved interface) was computed using the ANRAY software package (Gajewski & Pšenčík, 1990). 3-D ray tracing is used to calculate the two-point rays of the reflected P, S1, S2 and converted waves (nine elementary waves). S1 wave is slower than S2 wave. We then compute three-component ray-theory seismograms at the receivers. The advantage of the ray method is separate calculation of each component for each elementary wave.

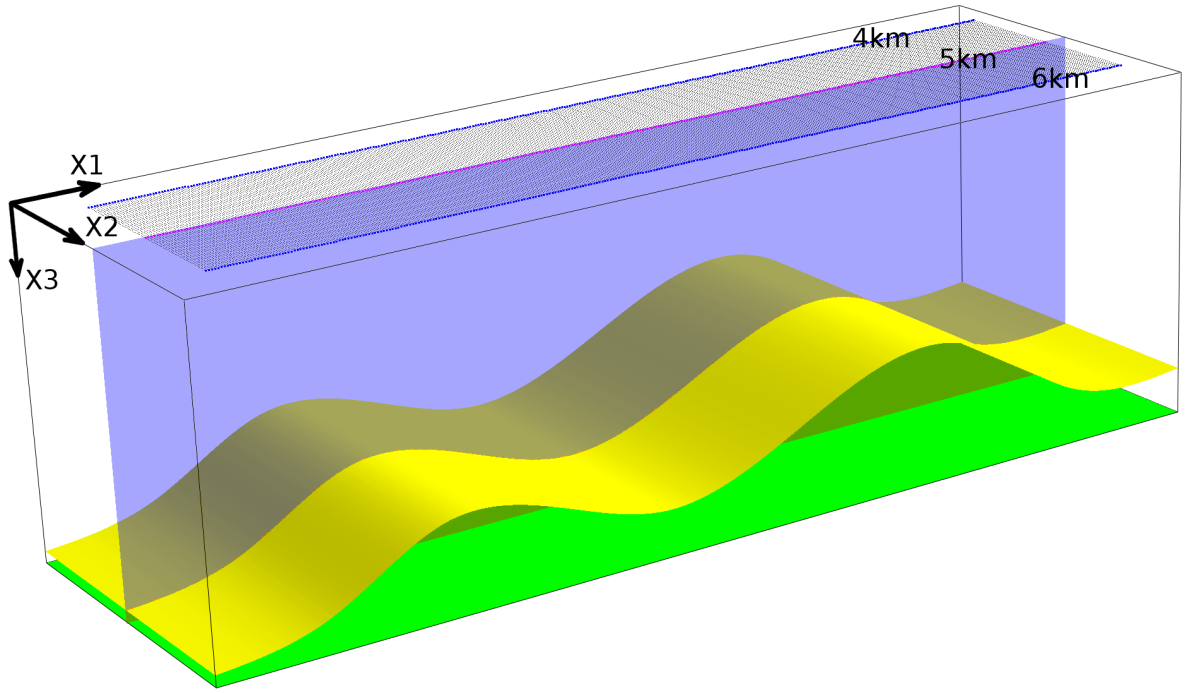

Figure 2. Part of the velocity model with 81 parallel profile lines, the curved interface (yellow) and the bottom velocity model plane (green). The horizontal dimensions of the depicted part of the velocity model are 0 km $\leq x_1 \leq$ 9.2 km, 3.5 km $\leq x_2 \leq$ 6.5 km, the depth is 0 km $\leq x_3 \leq$ 3 km. We compute and stack migrated sections in the 2-D plane (blue) located in the middle of the shot-receiver configuration, at horizontal coordinate $x_2 = 5$ km.

The recorded wave field is equal for all parallel profile lines, because the distribution of elastic moduli in each layer is homogeneous, and the non-inclined curved interface is independent of the coordinate x_2 perpendicular to the profile lines (2.5-D velocity model, see Figures 1 and 2).

The triclinic asymmetry causes that the two-point rays do not stay in the vertical planes corresponding to the individual profiles (see Figure 3).

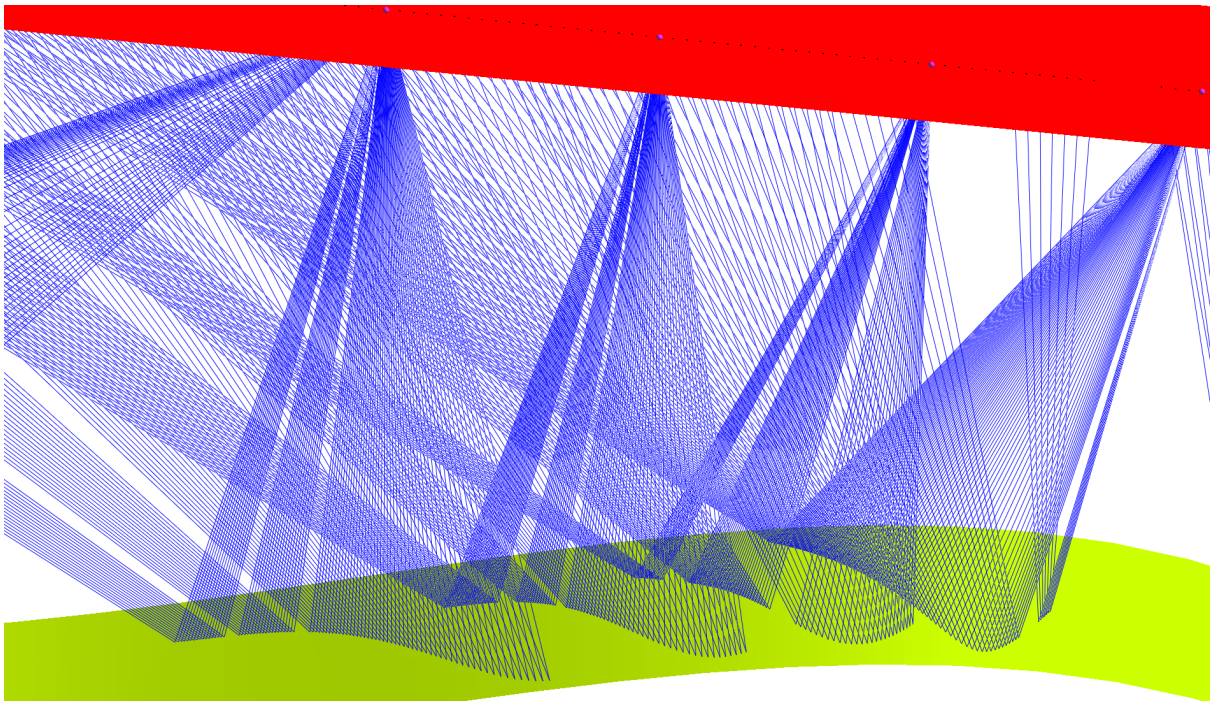

Figure 3. Detailed view of two-point rays of the reflected S1S2 wave for shots 80, 100, 120 and 140. Note the curved paths of reflections at the interface.

4.1 Ray-velocity surfaces

To see how complex is calculating ray-theory S1, S2 and converted waves, we generate and display the ray-velocity surfaces for the relatively strong triclinic anisotropy given by matrix (1). The ray-velocity surface (group-velocity surface, Fresnel wave surface) at spatial point x^m is composed of three sheets corresponding to the three eigenvalues of the Christoffel matrix (Klimeš, 2002).

While the ray-velocity surface of the P wave is convex and smooth (see Figure 4), the surfaces of the ray-theory S1 and S2 waves are much more complex (see Figures 5-9). The detailed study of S1 and S2 surfaces shows many common, singular points. Some parts of the ray-velocity S1 and S2 surfaces are concave or intersect. All these anomalies cause ray-theory calculation problems in some directions.

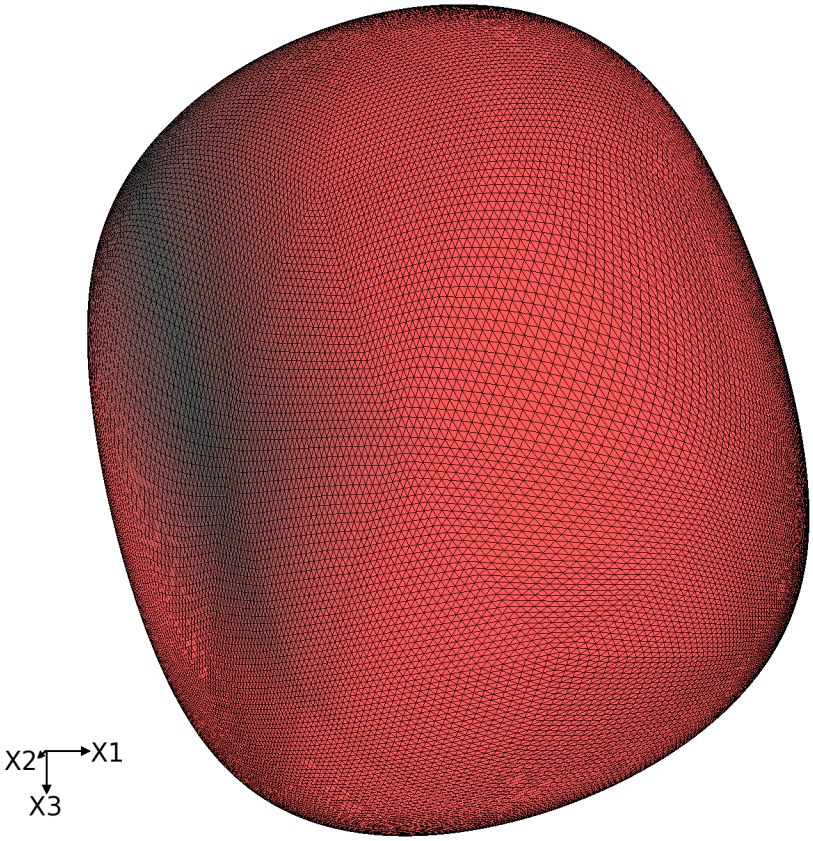

Figure 4. The **P** wave ray-velocity surface for the triclinic anisotropy.

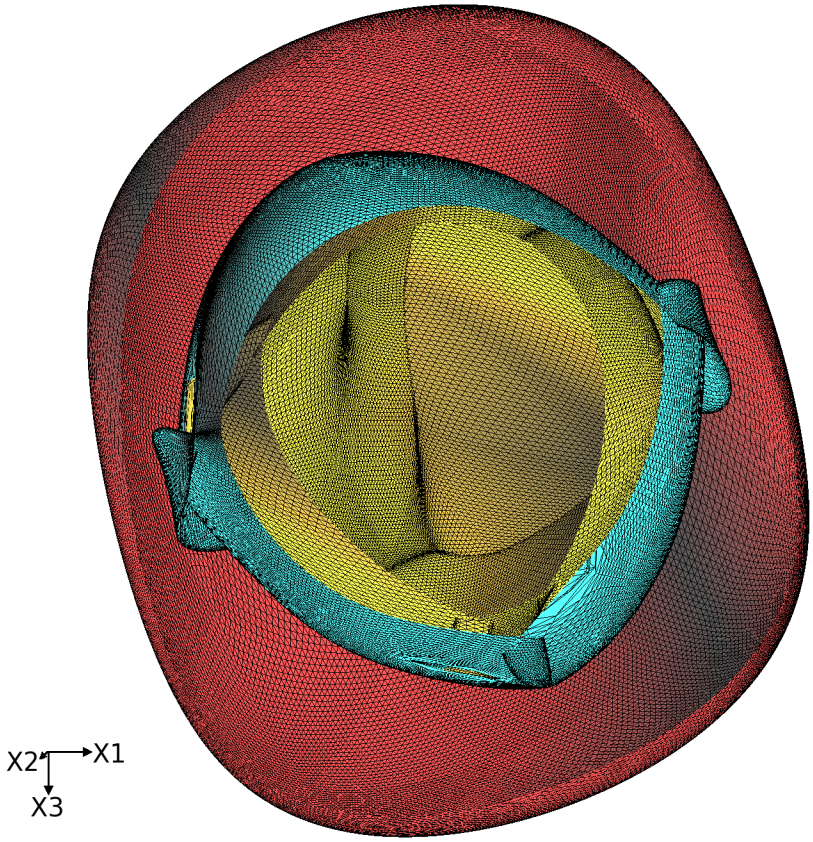

Figure 5. The sliced **P**, **S1** and **S2** wave ray-velocity surfaces for the triclinic anisotropy.

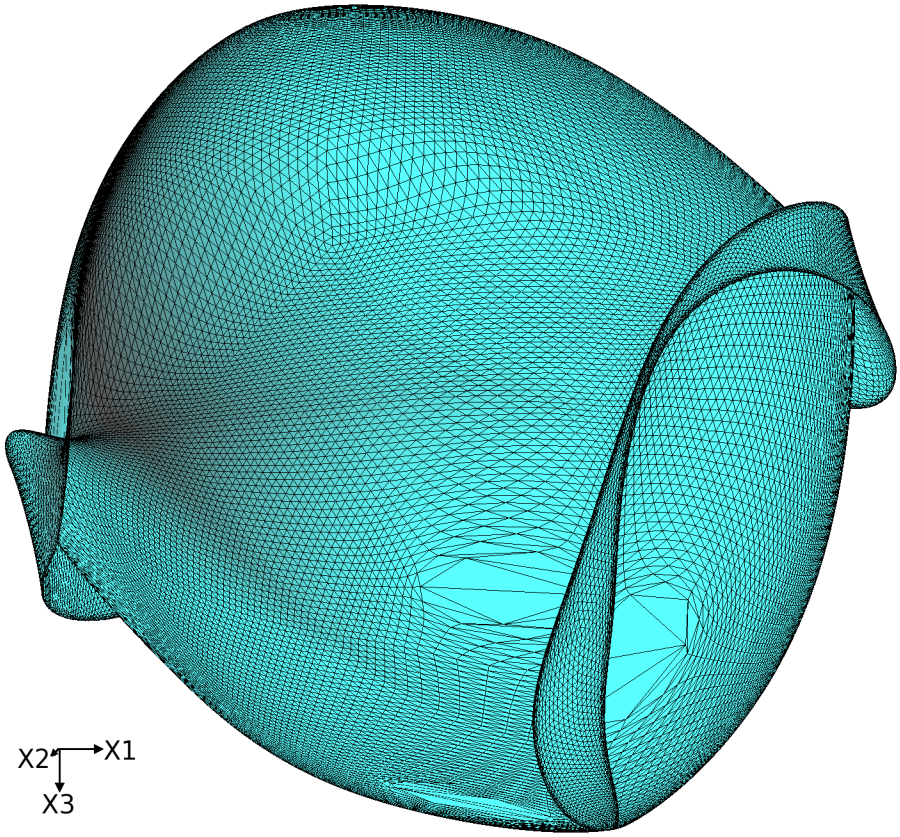

Figure 6. The S2 wave ray-velocity surface for the triclinic anisotropy.

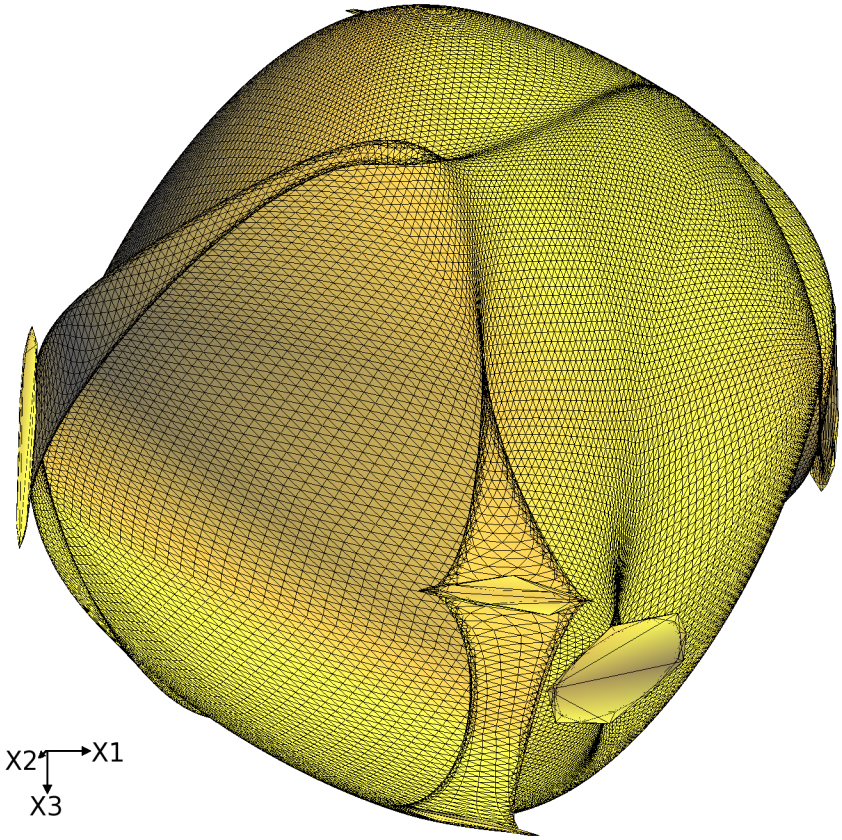

Figure 7. The S1 wave ray-velocity surface for the triclinic anisotropy.

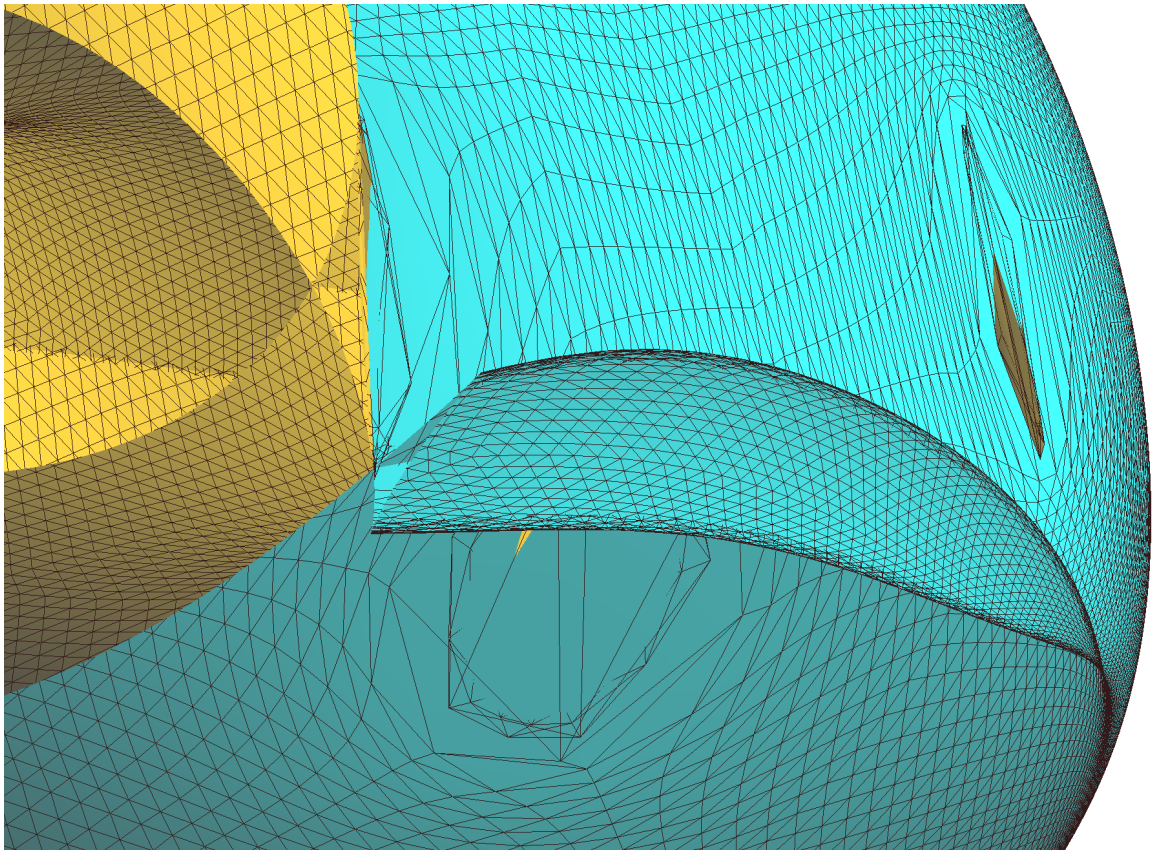

Figure 8. Detail of the sliced and rotated S1 and S2 wave ray-velocity surfaces for the triclinic anisotropy.

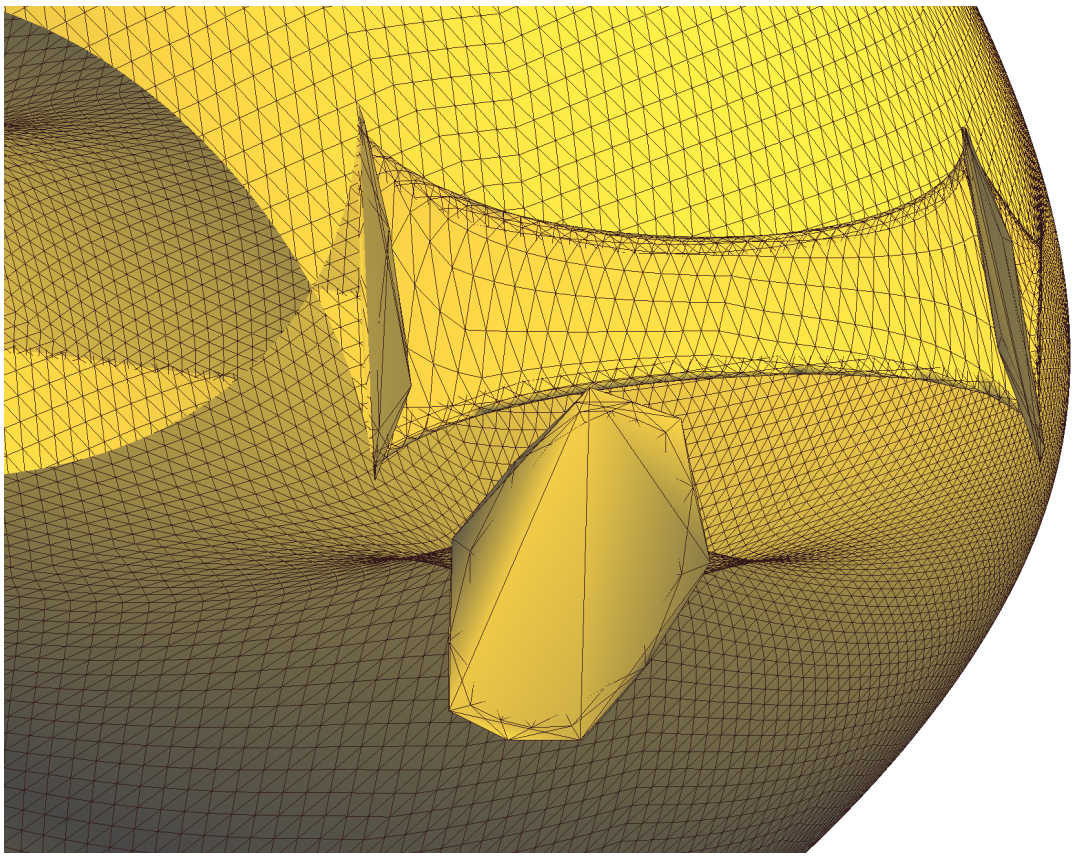

Figure 9. Detail of the sliced and rotated S1 wave ray-velocity surface for the triclinic anisotropy.

4.2 Synthetic seismograms

We use an explosive source for calculation of ray-theory synthetic seismograms. The source-time function is a Gabor wavelet, $\exp[-(2\pi f/\gamma)^2 2t^2]\cos(2\pi f t)$, with the dominant frequency $f = 25$ Hz and $\gamma = 1$.

The relatively strong triclinic anisotropy causes generation of strong S1, S2 and converted waves even for an explosive source (see Figures 10, 11 and 12).

For the P, S1, S2 and converted waves, we observe receivers with the change of the sign of the reflection coefficient around a region of the nearly vanishing reflection coefficient. This is caused by the fact that the value of the corresponding elementary wave velocity in the isotropic bottom layer is between the values of the horizontal (axis x_1) and vertical (axis x_3) wave velocities in anisotropic upper layer.

On the other hand, for S1, S2 and converted waves, we observe seismograms with enormous amplitudes for some shot-receiver configurations, caused probably by singularities.

Figure 10 shows radial components of the seismograms for 9 elementary reflected and converted waves for one selected shot-receiver configuration: PP wave, PS2 wave, PS1 wave, S2P wave, S1P wave, S2S2 wave, S1S2 wave, S2S1 wave and S1S1 wave. Notation is simple, the first letter denotes elementary wave from the source to the reflection point and the second letter denotes elementary wave from the reflection point to the receiver. P is for P wave, S1 and S2 are for ray-theory S waves.

Analogously Figures 11 and 12 display transversal and vertical components of seismograms for 9 elementary reflected and converted waves for one selected shot-receiver configuration. All seismograms in Figures 10, 11 and 12 have the same scaling.

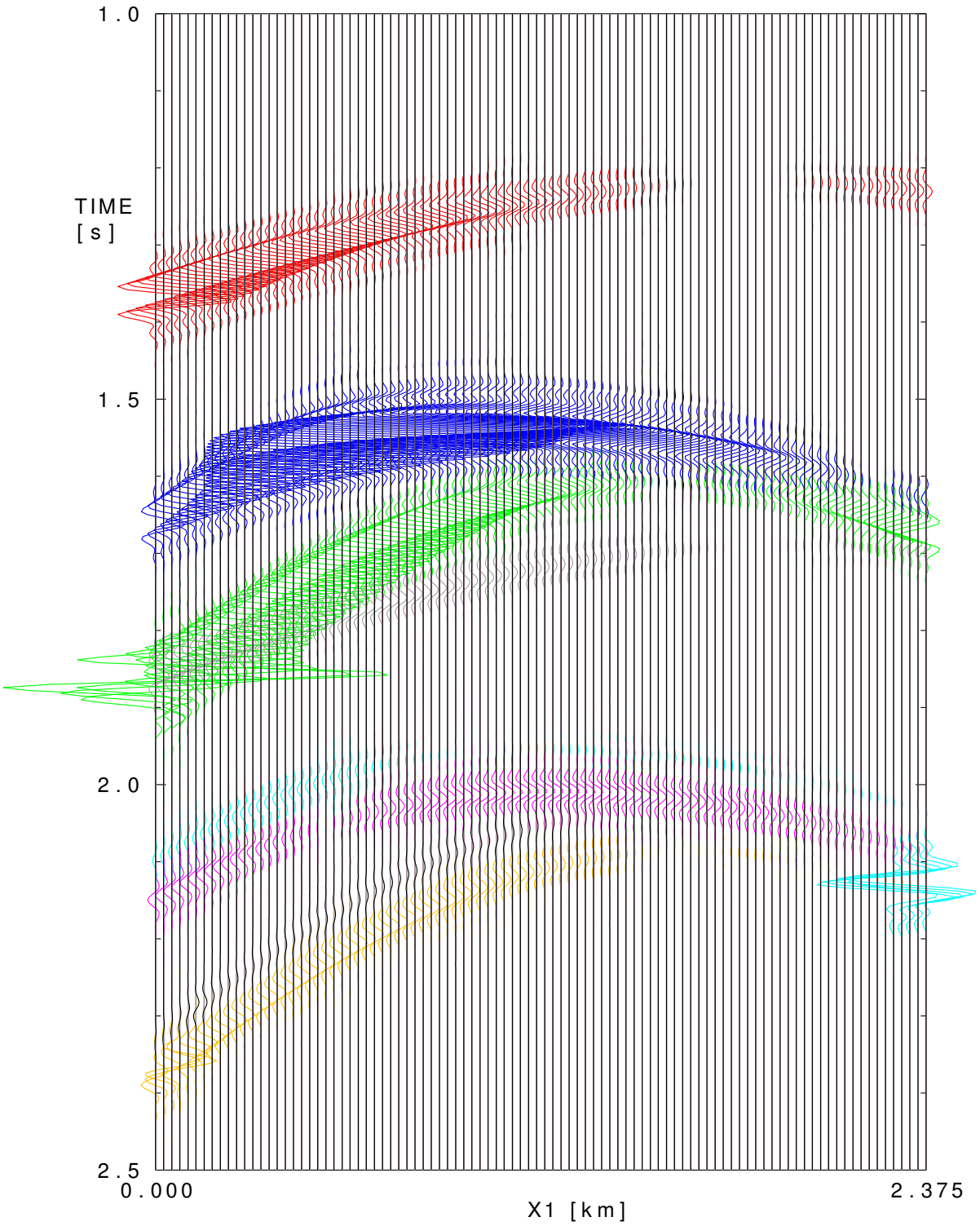

Figure 10. Radial component (X1) of the synthetic seismograms of the reflected P, S1, S2 and converted waves for the single common-shot gather at line $x_2 = 5$ km corresponding to shot 20 ($x_1 = 3.475$ km). The 9 elementary waves, ordered approximately according to travel time from the smallest, are **PP** wave, **PS2** wave, **PS1** wave, **S2P** wave (nearly invisible), **S1P** wave, **S2S2** wave, **S1S2** wave, **S2S1** wave (poorly visible) and **S1S1** wave. All seismograms have the same scaling.

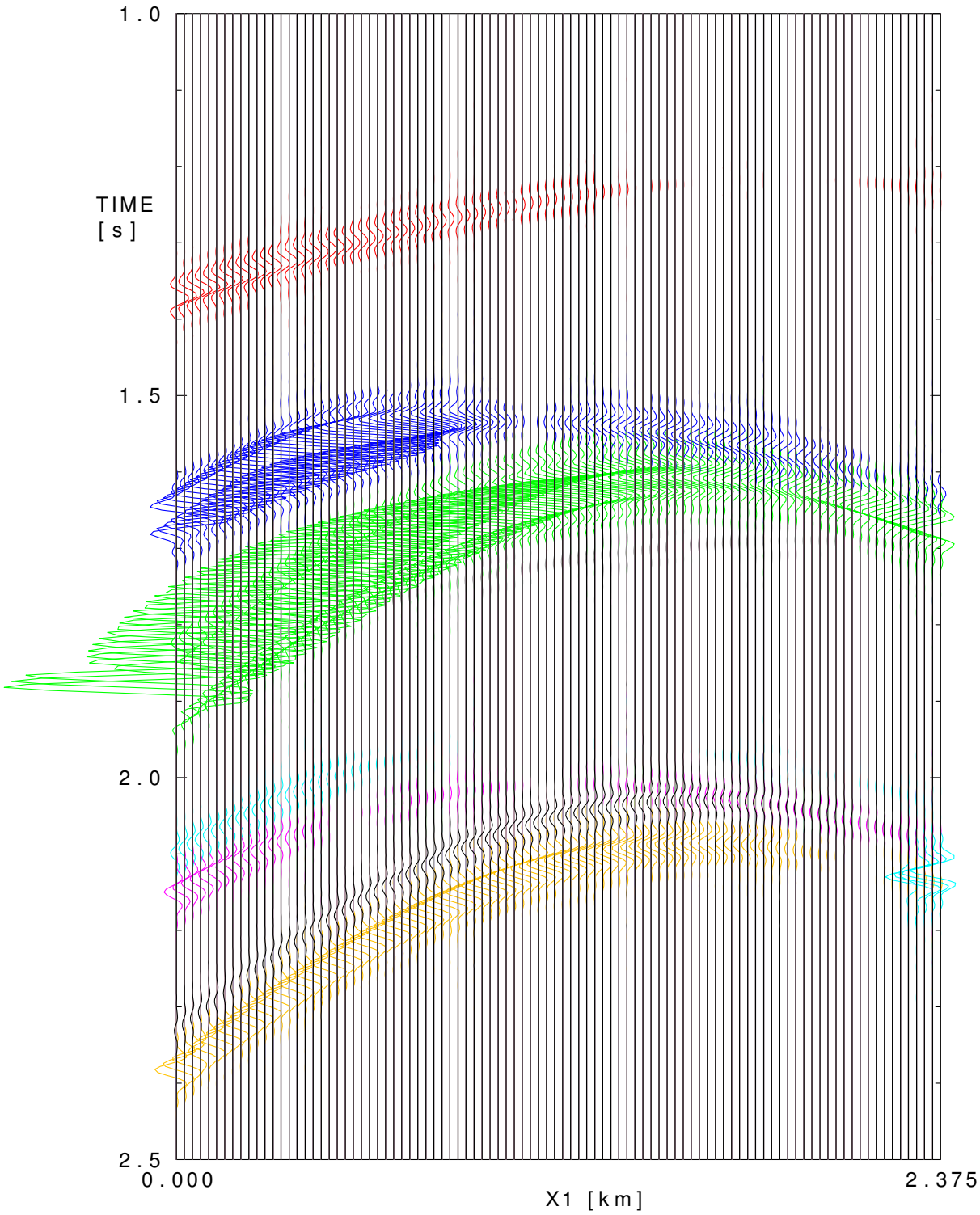

Figure 11. Transversal component (X2) of the synthetic seismograms of the reflected P, S1, S2 and converted waves for the single common-shot gather at line $x_2 = 5$ km corresponding to shot 20 ($x_1 = 3.475$ km). The 9 elementary waves, ordered approximately according to travel time from the smallest, are **PP** wave, **PS2** wave, **PS1** wave, **S2P** wave (nearly invisible), **S1P** wave, **S2S2** wave, **S1S2** wave, **S2S1** wave (poorly visible) and **S1S1** wave. All seismograms have the same scaling.

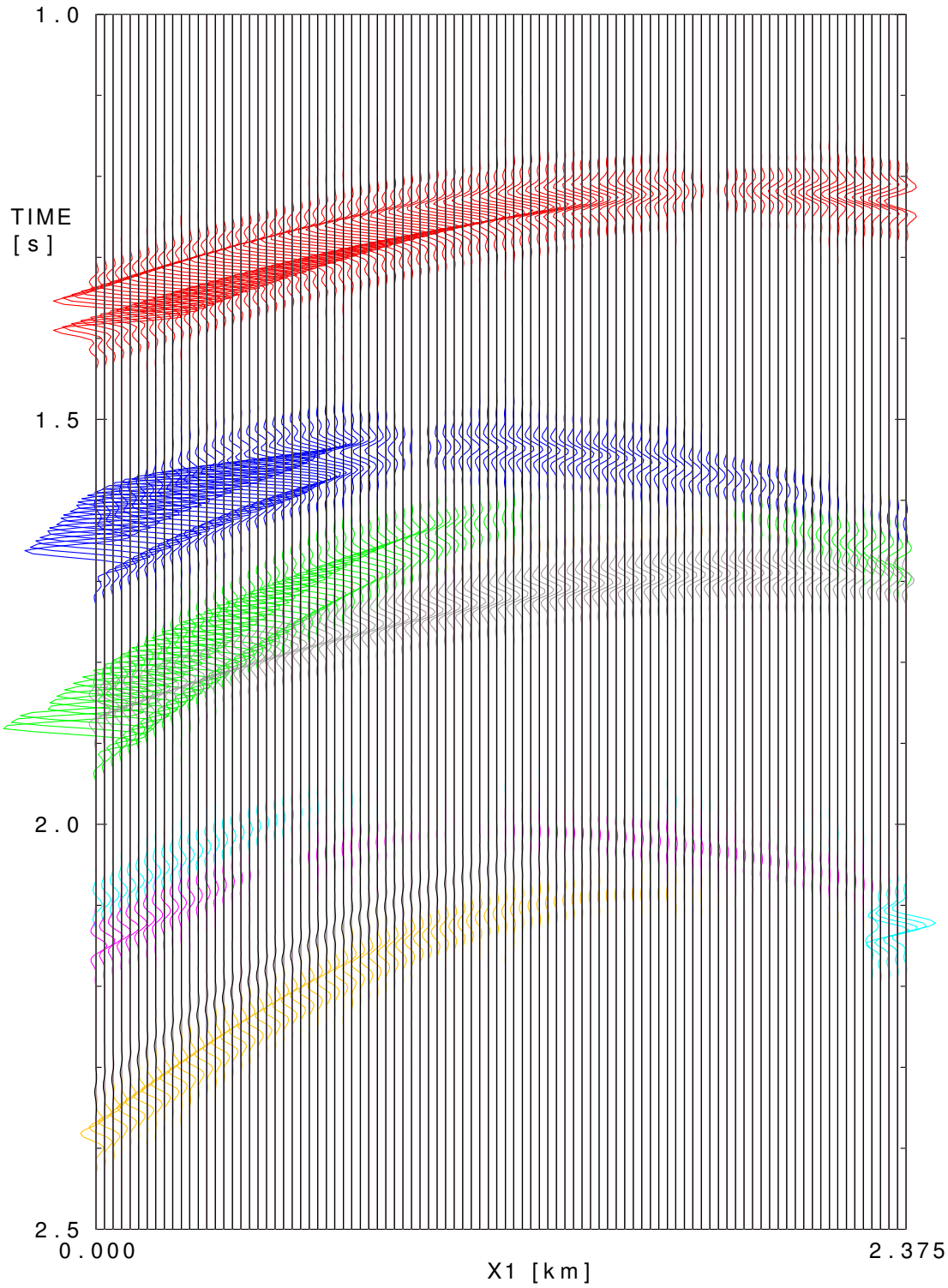

Figure 12. Vertical component (X3) of the synthetic seismograms of the reflected P, S1, S2 and converted waves for the single common-shot gather at line $x_2 = 5$ km corresponding to shot 20 ($x_1 = 3.475$ km). The 9 elementary waves, ordered approximately according to travel time from the smallest, are **PP** wave, **PS2** wave, **PS1** wave, **S2P** wave (nearly invisible), **S1P** wave, **S2S2** wave, **S1S2** wave, **S2S1** wave (poorly visible) and **S1S1** wave. All seismograms have the same scaling.

5. Kirchhoff prestack depth scalar migration

We use the MODEL, CRT, FORMS and DATA software packages for the 3-D Kirchhoff prestack depth scalar migration (Červený, Klimeš & Pšenčík, 1988; Bulant, 1996; Bucha & Bulant, 2017). We migrate separately individual components of individual waves. The migration of each component separately means that we migrate only a specific portion of the wave field corresponding to a specific portion of the migrated interface.

The migration consists of two-parametric controlled initial-value ray tracing (Bulant, 1999) from the individual surface points, calculating grid values of travel times and amplitudes by interpolation within ray cells (Bulant & Klimeš, 1999), performing the common-shot migration and stacking the migrated images. The shot-receiver configuration consists of 81 parallel profile lines at intervals of 0.025 km (see Figure 2). The first profile line is situated at horizontal coordinate $x_2 = 4$ km and the last profile line is situated at horizontal coordinate $x_2 = 6$ km. For migration we use the single-layer velocity model (without the curved interface) with the same triclinic anisotropy as in the upper layer of the velocity model used to calculate the recorded wave field given by matrix (1).

In our tests, we calculate only one vertical image section corresponding to the central profile line ($x_2 = 5$ km, see Figure 2). Although it is only a 2-D profile line, such an image represents one vertical section of full 3-D migrated volume. We form the image by computing and summing the corresponding contributions (images) from all 81 parallel source-receiver lines. While summing the contributions, the constructive interference focuses the migrated interface and the destructive interference reduces undesirable migration artefacts (non-specular reflections). We also use cosine taper to clear artefacts, but some of them, especially residual semicircular smiles, remain.

During calculations, we encounter problems with anomalous amplitudes of the Green function for S1S1, S2S2, S1S2, S2S1, PS1 and PS2 waves caused by singularities for some common-shot gathers. These anomalies yield additional migration artefacts (noise). We solved the problem by limiting the maximum value of the Green function.

Figure 13 shows stacked migrated sections calculated separately for radial, transversal and vertical components of reflected PP wave. The migrated interface is clear and coincides nearly perfectly with the interface in the velocity model used to compute the recorded wave field.

Analogously, Figures 14-17 show stacked migrated sections calculated separately for three components of the reflected ray-theory S1S1, S2S2, S1S2 and S2S1 elementary waves. The results are worse than for the PP wave.

Some parts of migrated interface are poorly imaged. We see differences among individual components for individual elementary waves. The poorly imaged parts of interface are probably caused by ray-theory complex synthetic wave field. Amplitudes of the wave field are influenced by the change of the sign of the reflection coefficient around a region of the nearly vanishing reflection coefficient. This is caused by the fact that the value of the corresponding elementary wave velocity in isotropic bottom layer is between the values of the horizontal (axis x_1) and vertical (axis x_3) wave velocities in anisotropic upper layer. On the other side, we observe some short parts of the wave field with enormous amplitudes for some shot-receiver configurations, caused probably by singularities. Anomalies of the ray-velocity S1 and S2 surfaces cause ray-theory calculation problems in some directions (missing rays).

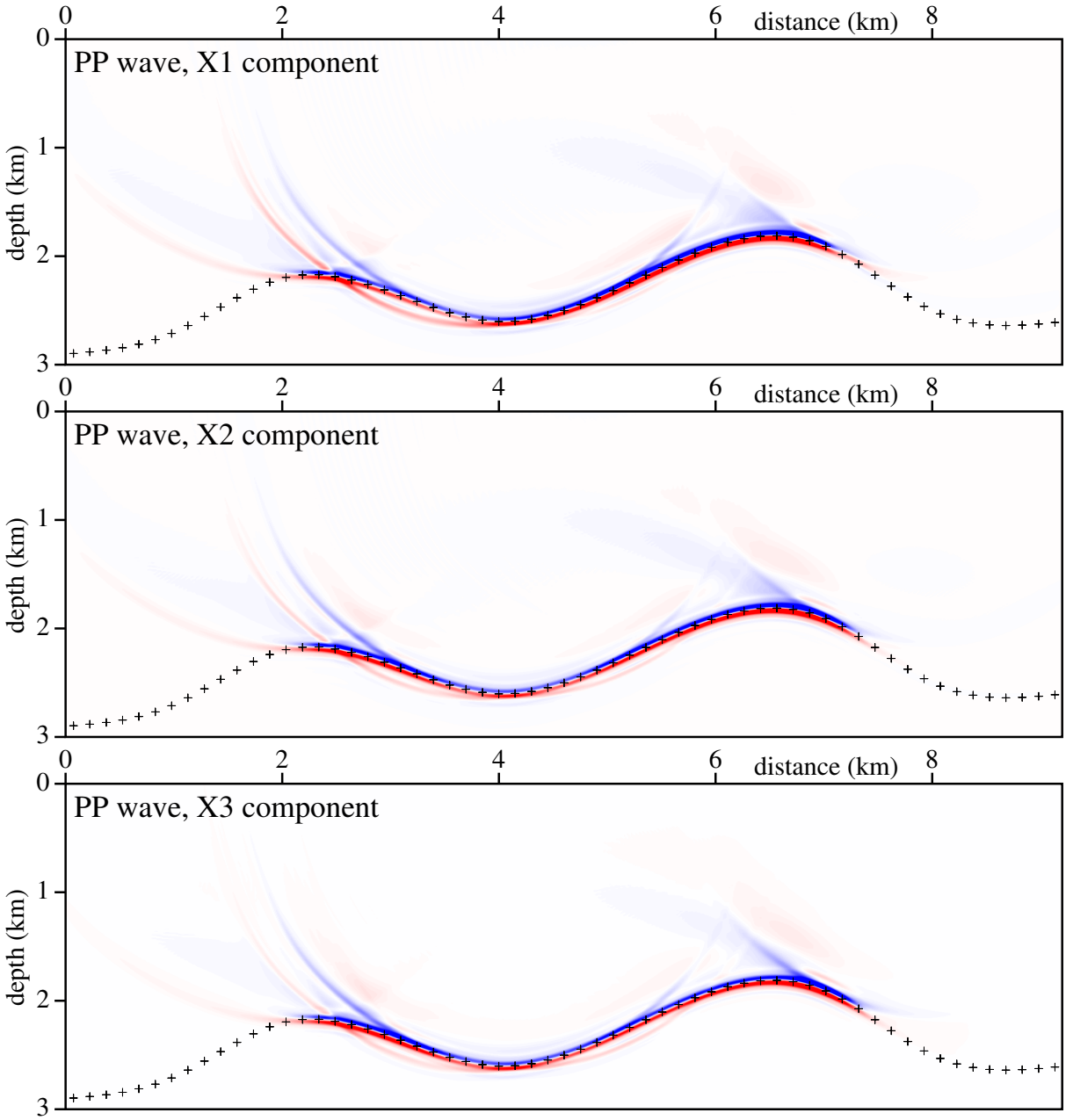

Figure 13. Stacked migrated sections calculated in the triclinic velocity model without interface. Radial (X1), transversal (X2) and vertical (X3) components of PP reflected wave are used. The elastic moduli in the single-layer velocity model for migration are the same as in the upper layer of the velocity model used to calculate the recorded wave field. 81×240 common-shot prestack depth migrated sections, corresponding to 81 profile lines and 240 sources along each profile line, have been stacked. The crosses denote the interface in the velocity model used to compute the recorded wave field.

Note several combinations of reverse amplitudes in migrated sections for S1S1, S2S2, S1S2 and S2S1 elementary waves. For example, radial (X1) component has reverse amplitudes than transversal (X2) and vertical (X3) components of S1S1 wave (see Figure 14). Vertical components (X3) for S1S1, S1S2 waves have reverse amplitudes with respect to S2S2, S2S1 waves (see Figures 14-17). Moreover, some parts of the same migrated interface have alternating amplitudes (see Figure 16). The summation of all sections thus might diminish the result.

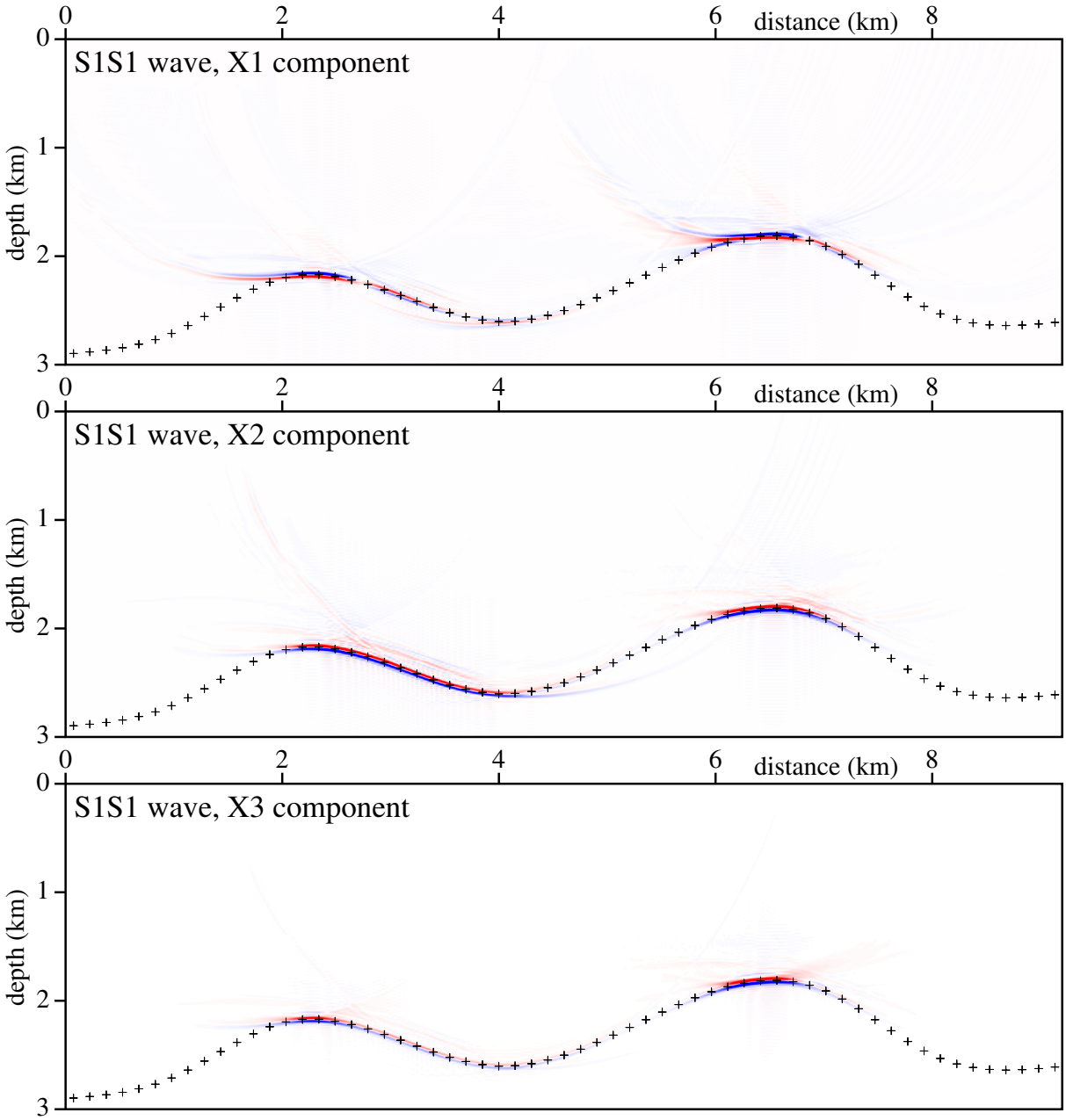

Figure 14. Stacked migrated sections calculated in the triclinic velocity model without interface. Radial (X1), transversal (X2) and vertical (X3) components of S1S1 reflected wave are used. The elastic moduli in the single-layer velocity model for migration are the same as in the upper layer of the velocity model used to calculate the recorded wave field. 81×240 common-shot prestack depth migrated sections, corresponding to 81 profile lines and 240 sources along each profile line, have been stacked. The crosses denote the interface in the velocity model used to compute the recorded wave field.

Migrated interfaces for transversal (X2) component of PS1 converted wave (see Figure 18) and for radial (X1) component of PS2 converted wave (see Figure 19) are clear and coincide nearly perfectly with the interface in the velocity model used to compute the recorded wave field. All other migrated interfaces for other components of converted PS1, PS2, S1P and S2P elementary waves have some parts of the migrated sections poorly imaged (see Figures 18-21). Similarly to reflected S1 and S2 waves, note several combinations of reverse migration amplitudes. Several migrated sections contain strong migration artefacts, smiles, that will be subject of further study.

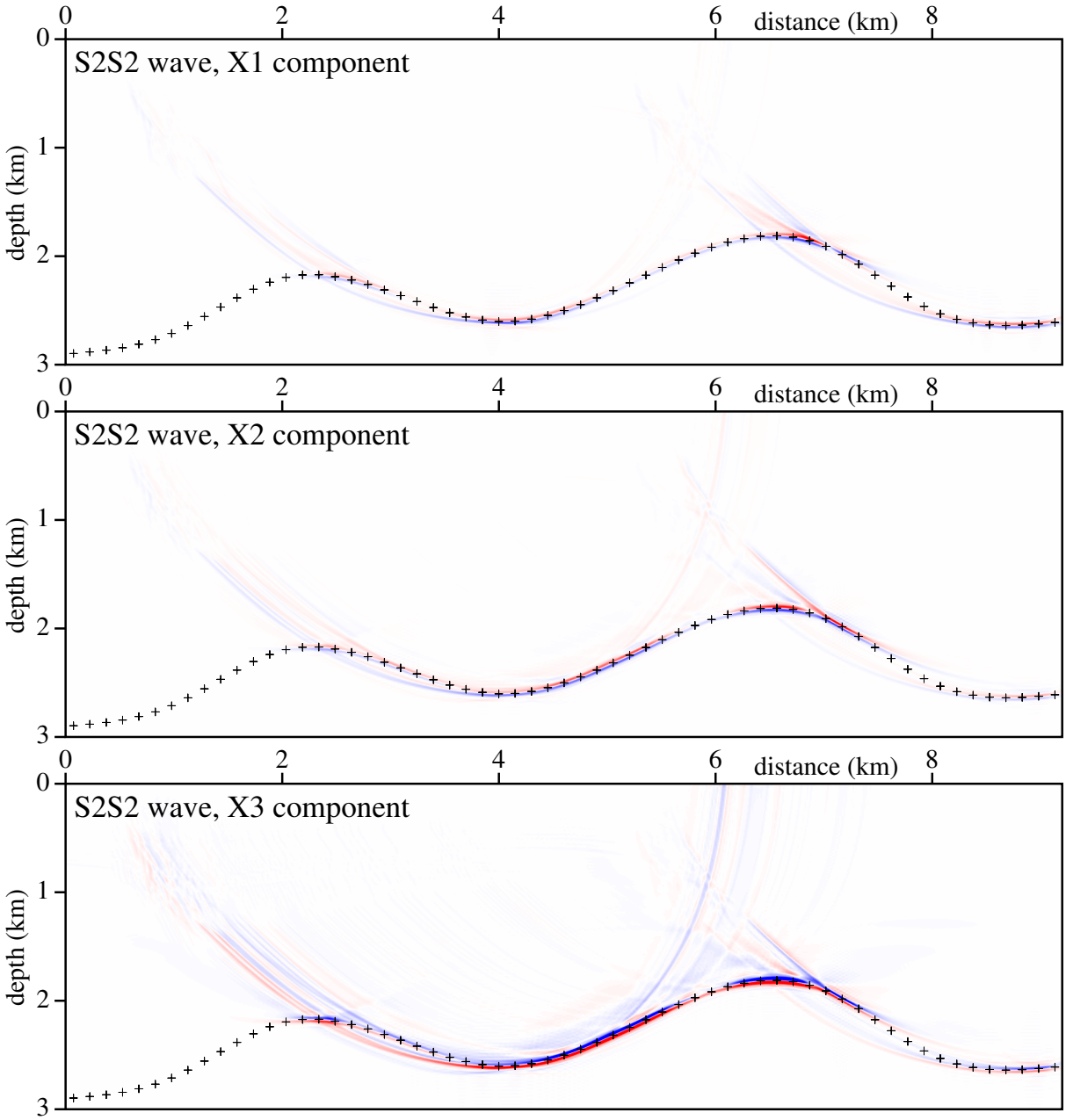

Figure 15. Stacked migrated sections calculated in the triclinic velocity model without interface. Radial (X1), transversal (X2) and vertical (X3) components of S2S2 reflected wave are used. The elastic moduli in the single-layer velocity model for migration are the same as in the upper layer of the velocity model used to calculate the recorded wave field. 81×240 common-shot prestack depth migrated sections, corresponding to 81 profile lines and 240 sources along each profile line, have been stacked. The crosses denote the interface in the velocity model used to compute the recorded wave field.

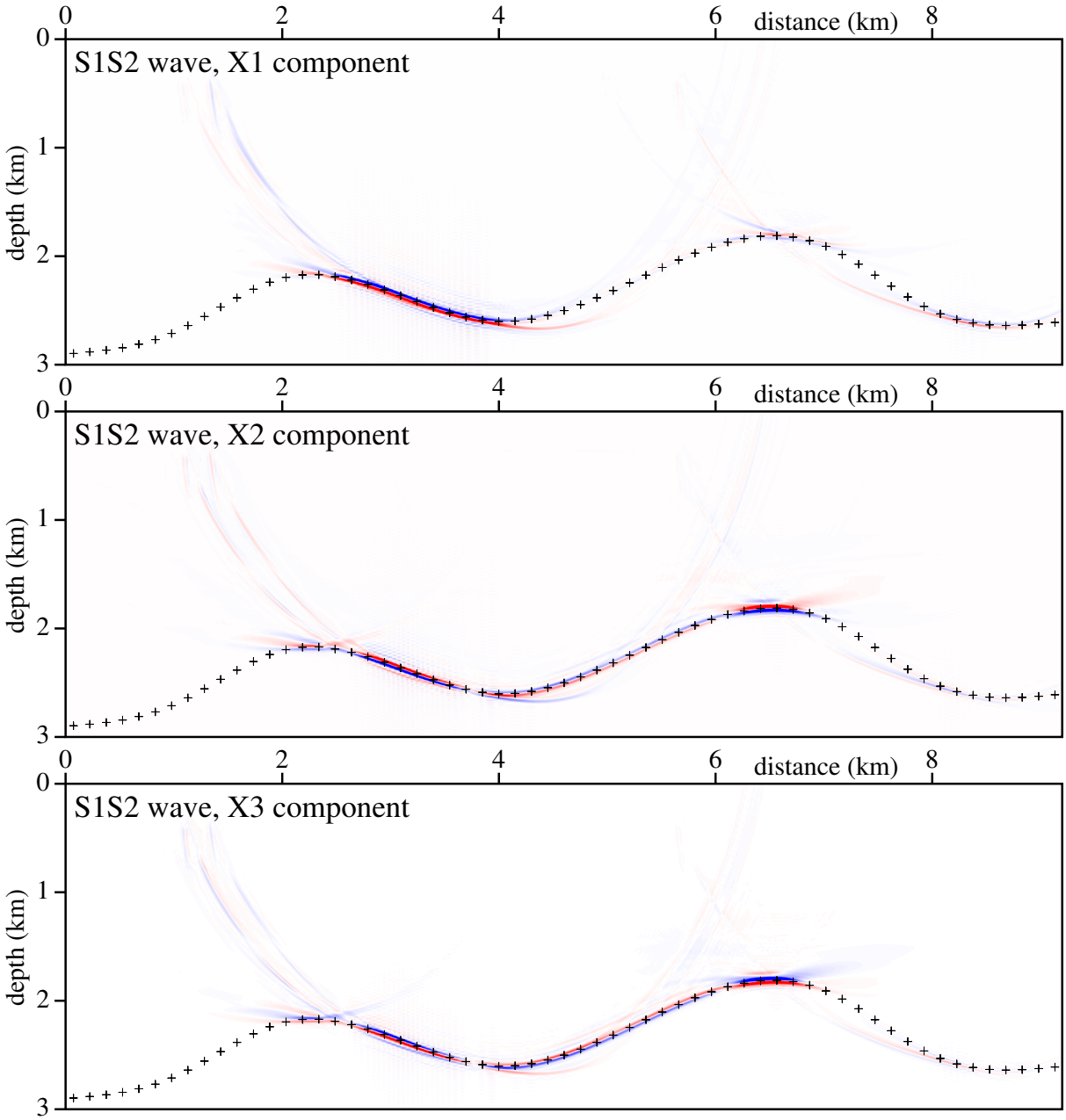

Figure 16. Stacked migrated sections calculated in the triclinic velocity model without interface. Radial (X1), transversal (X2) and vertical (X3) components of S1S2 reflected wave are used. The elastic moduli in the single-layer velocity model for migration are the same as in the upper layer of the velocity model used to calculate the recorded wave field. 81 × 240 common-shot prestack depth migrated sections, corresponding to 81 profile lines and 240 sources along each profile line, have been stacked. The crosses denote the interface in the velocity model used to compute the recorded wave field.

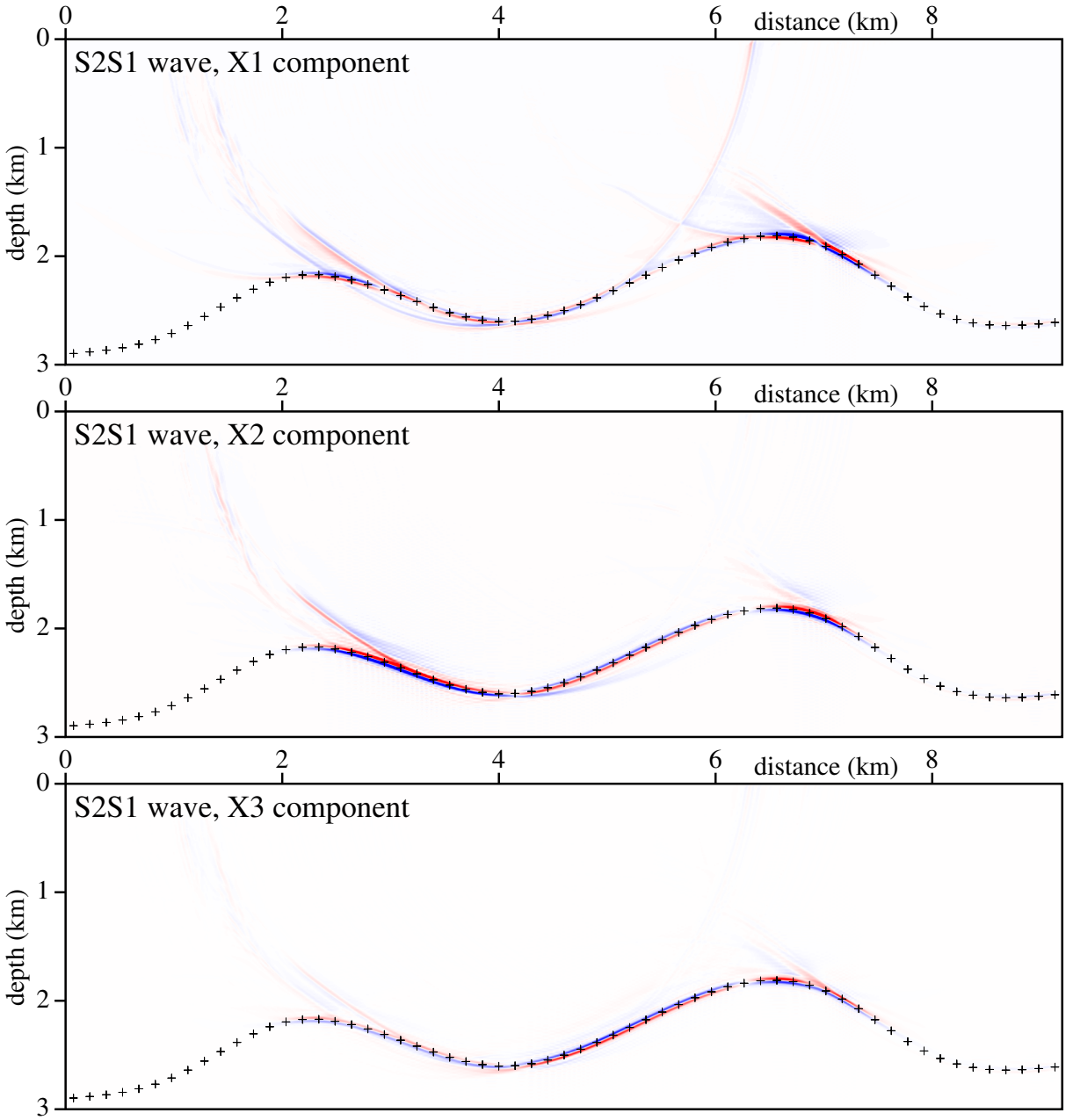

Figure 17. Stacked migrated sections calculated in the triclinic velocity model without interface. Radial (X1), transversal (X2) and vertical (X3) components of S2S1 reflected wave are used. The elastic moduli in the single-layer velocity model for migration are the same as in the upper layer of the velocity model used to calculate the recorded wave field. 81 × 240 common-shot prestack depth migrated sections, corresponding to 81 profile lines and 240 sources along each profile line, have been stacked. The crosses denote the interface in the velocity model used to compute the recorded wave field.

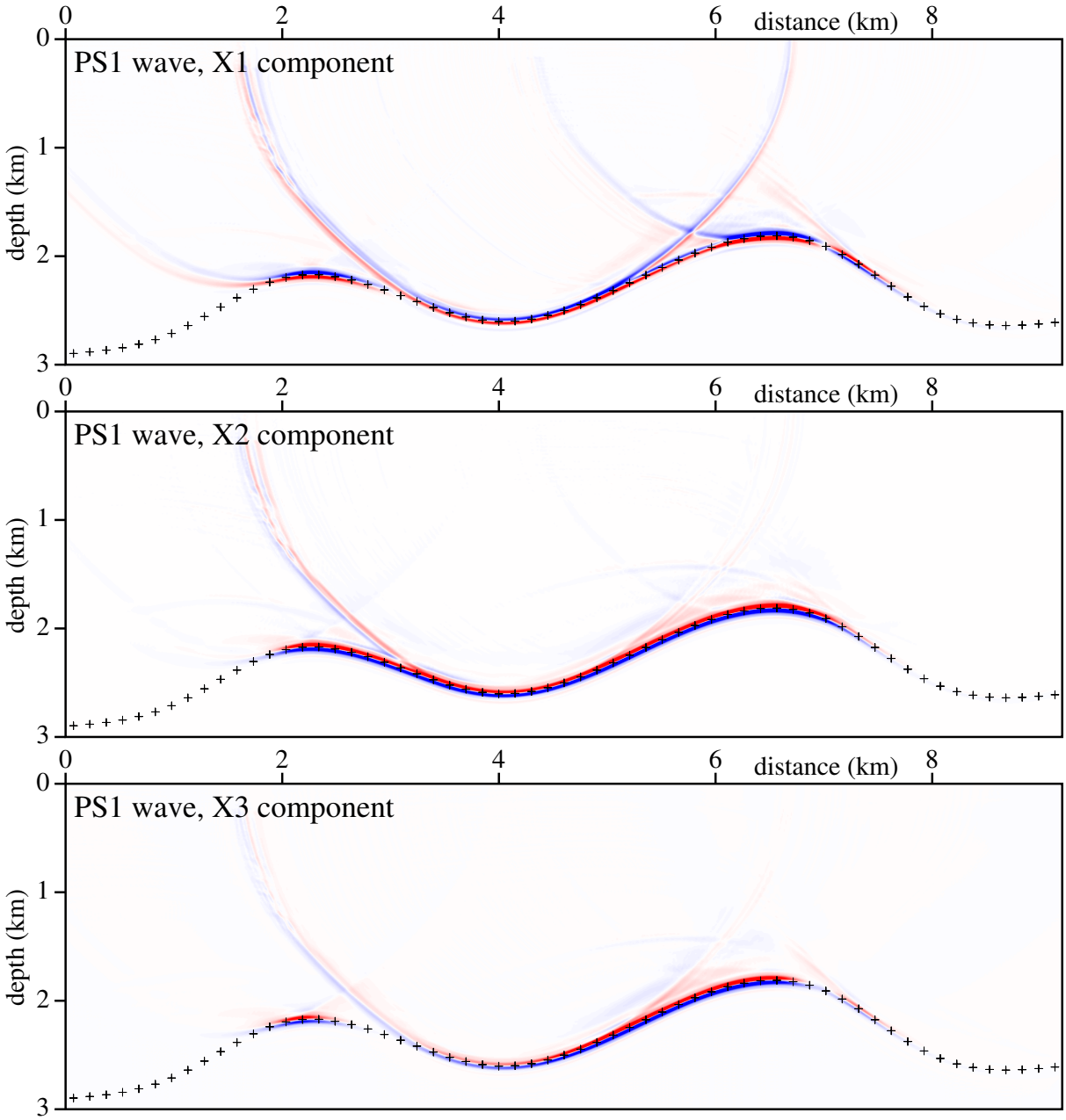

Figure 18. Stacked migrated sections calculated in the triclinic velocity model without interface. Radial (X1), transversal (X2) and vertical (X3) components of PS1 converted wave are used. The elastic moduli in the single-layer velocity model for migration are the same as in the upper layer of the velocity model used to calculate the recorded wave field. 81×240 common-shot prestack depth migrated sections, corresponding to 81 profile lines and 240 sources along each profile line, have been stacked. The crosses denote the interface in the velocity model used to compute the recorded wave field.

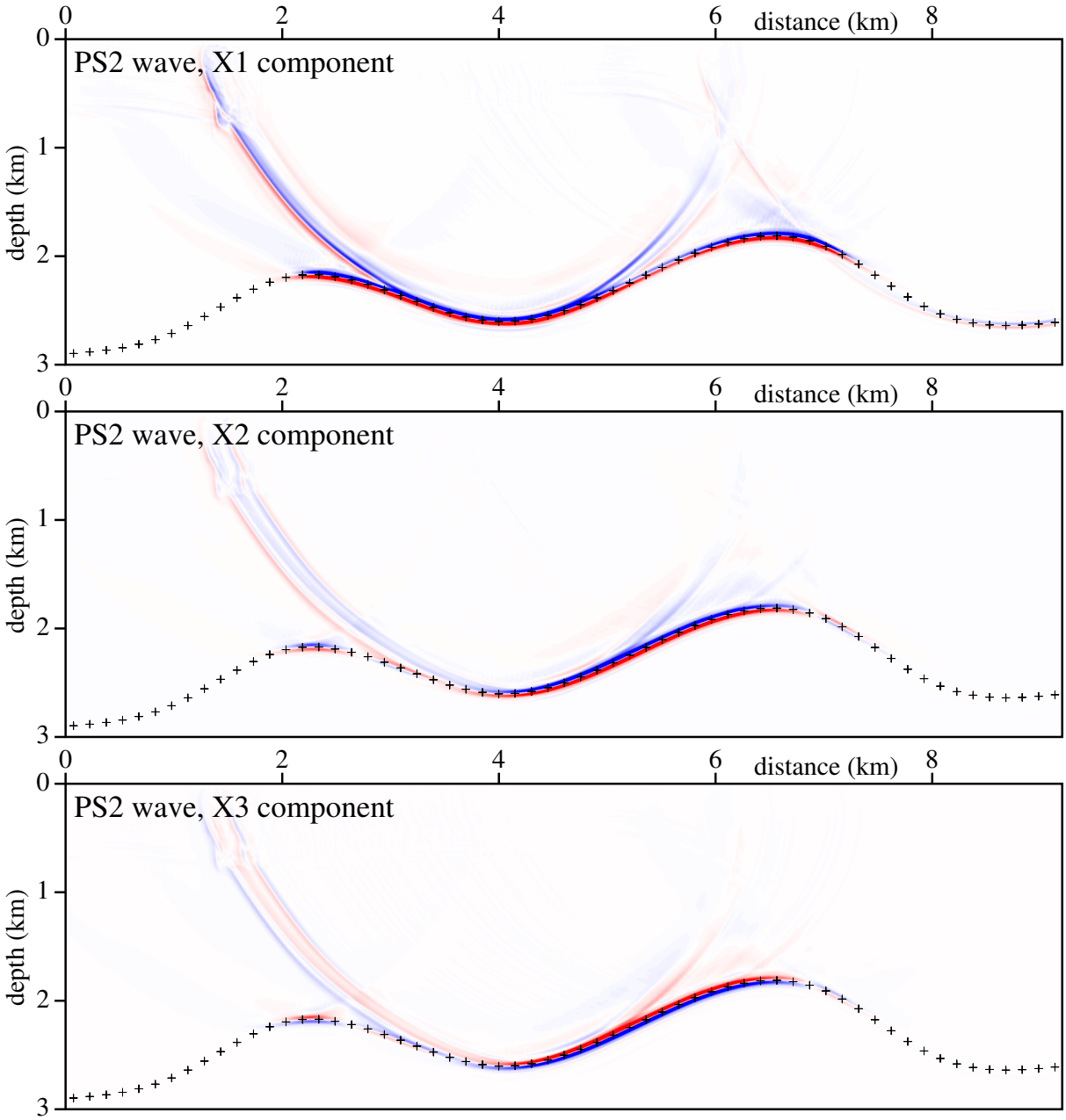

Figure 19. Stacked migrated sections calculated in the triclinic velocity model without interface. Radial (X1), transversal (X2) and vertical (X3) components of PS2 converted wave are used. The elastic moduli in the single-layer velocity model for migration are the same as in the upper layer of the velocity model used to calculate the recorded wave field. 81×240 common-shot prestack depth migrated sections, corresponding to 81 profile lines and 240 sources along each profile line, have been stacked. The crosses denote the interface in the velocity model used to compute the recorded wave field.

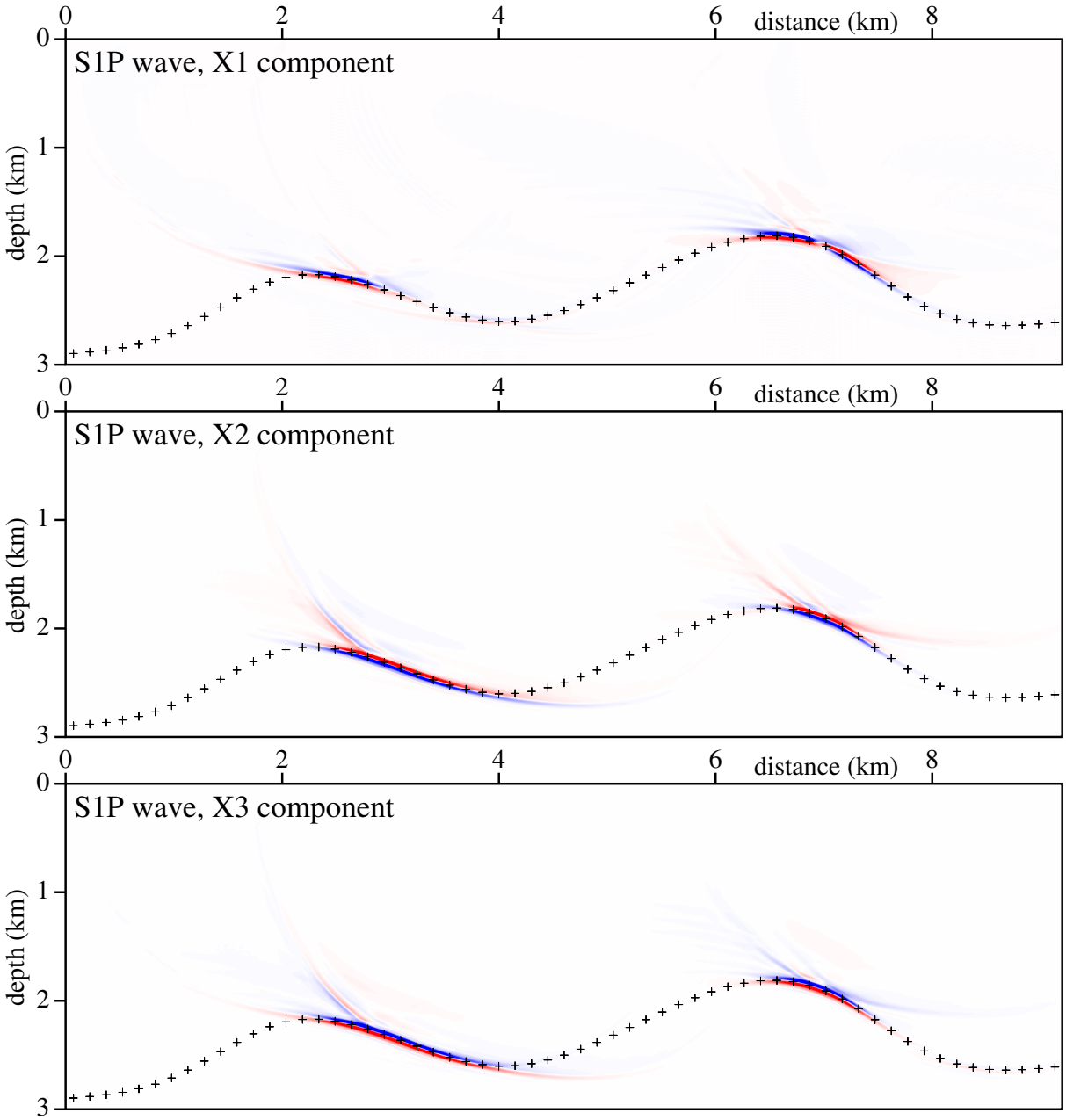

Figure 20. Stacked migrated sections calculated in the triclinic velocity model without interface. Radial (X1), transversal (X2) and vertical (X3) components of S1P converted wave are used. The elastic moduli in the single-layer velocity model for migration are the same as in the upper layer of the velocity model used to calculate the recorded wave field. 81 × 240 common-shot prestack depth migrated sections, corresponding to 81 profile lines and 240 sources along each profile line, have been stacked. The crosses denote the interface in the velocity model used to compute the recorded wave field.

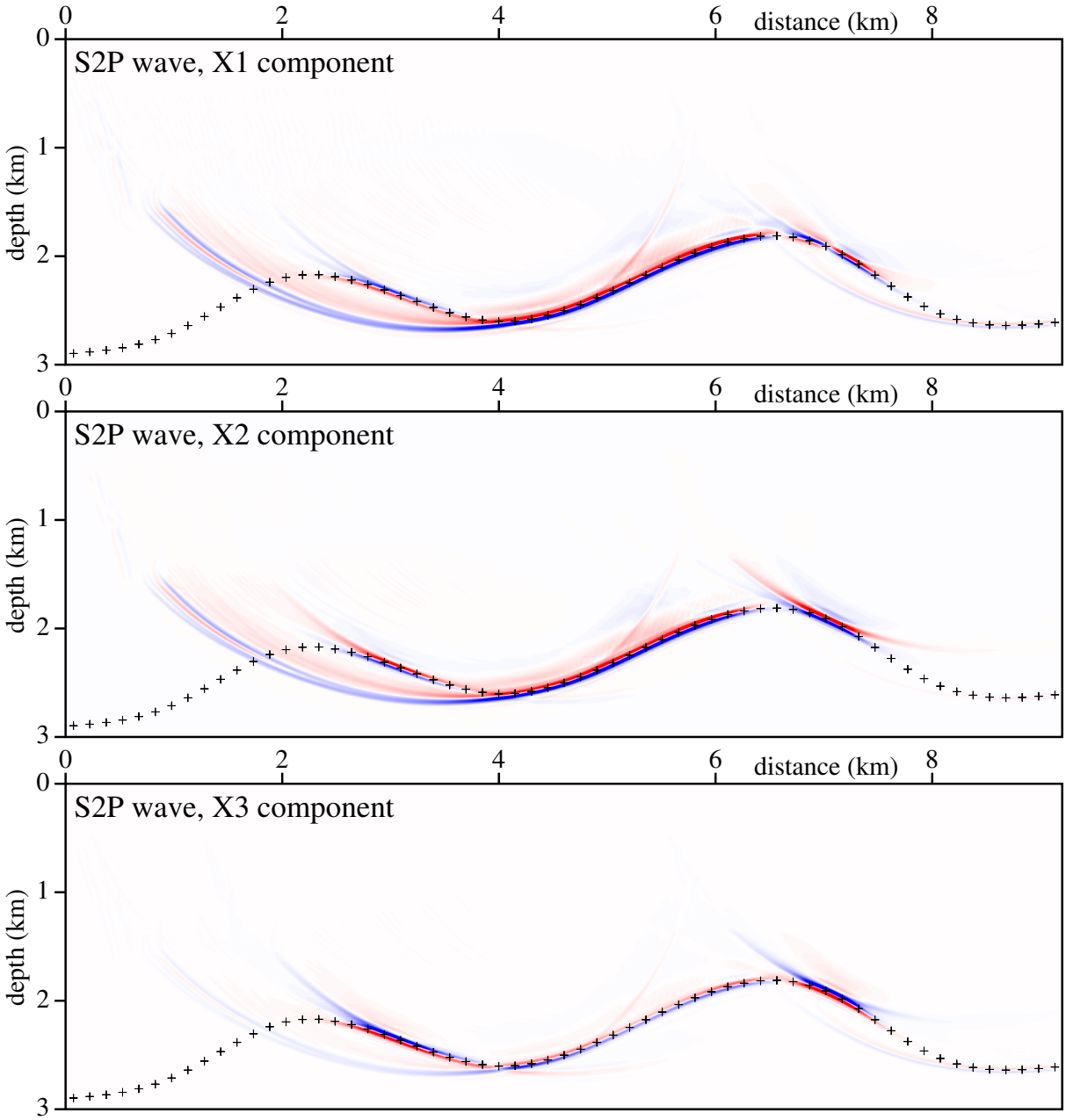

Figure 21. Stacked migrated sections calculated in the triclinic velocity model without interface. Radial (X1), transversal (X2) and vertical (X3) components of S2P converted wave are used. The elastic moduli in the single-layer velocity model for migration are the same as in the upper layer of the velocity model used to calculate the recorded wave field. 81 × 240 common-shot prestack depth migrated sections, corresponding to 81 profile lines and 240 sources along each profile line, have been stacked. The crosses denote the interface in the velocity model used to compute the recorded wave field.

6. Conclusions

We generated three-component synthetic seismograms of P, S1, S2 and converted waves using the ray theory in a simple two-layer velocity model composed of two homogeneous layers with relatively strong triclinic anisotropy in the upper layer. We then applied the 3-D ray-based Kirchhoff prestack depth scalar migration to the homogeneous single-layer velocity model with the same triclinic anisotropy. We migrated individual components of individual elementary waves separately.

The migrated interface is clear and coincides nearly perfectly with the interface in the velocity model used to compute the recorded wave field for:

- radial, transversal and vertical components of reflected PP wave,
- transversal component of PS1 converted wave,
- radial component of PS2 converted wave.

The quality of migrated sections for other elementary waves fluctuates. Some parts of the migrated interface are imaged clearly, some poorly. The poorly imaged parts of interface are probably caused by:

- the change of the sign of the reflection coefficient around regions of the nearly vanishing reflection coefficient,
- anomalies of the ray-velocity S1 and S2 surfaces.

Moreover, there are migrated interfaces for S1, S2 and converted waves with reverse amplitudes caused by the migration of individual components. The summation of migrated sections thus might diminish the result. Detailed reasons of calculation problems and change to vector migration instead of scalar approach will be subject of further study.

Acknowledgements

The author thanks Luděk Klimeš and Ivan Pšenčík for their help throughout the work on this paper.

The research has been supported by the Grant Agency of the Czech Republic under Contract 16-05237S, by the Ministry of Education of the Czech Republic within Research Project CzechGeo/EPOS LM2015079, and by the members of the consortium "Seismic Waves in Complex 3-D Structures" (see "http://sw3d.cz").

References

Bucha, V. (2012): Kirchhoff prestack depth migration in 3-D simple models: comparison of triclinic anisotropy with simpler anisotropies. *Stud. geophys. geod.*, **56**, 533–552. https://doi.org/10.1007/s11200-011-0253-5

Bucha, V. (2013): Kirchhoff prestack depth migration in velocity models with and without vertical gradients: Comparison of triclinic anisotropy with simpler anisotropies. *Seismic Waves in Complex 3-D Structures*, **23**, 45–59, online at "http://sw3d.cz".

Bucha, V. (2017): Kirchhoff prestack depth migration in simple models with differently rotated elasticity tensor: orthorhombic and triclinic anisotropy. *J. seism. Explor.*, **26**, 1–24.

Bucha, V. & Bulant, P. (eds.) (2017): SW3D-CD-21 (DVD-ROM). *Seismic Waves in Complex 3-D Structures*, **27**, 133–134, online at "http://sw3d.cz".

Bulant, P. (1996): Two-point ray tracing in 3-D. *Pure appl. Geophys.*, **148**, 421–447. https://doi.org/10.1007/BF00874574

Bulant, P. (1999): Two-point ray-tracing and controlled initial-value ray-tracing in 3-D heterogeneous block structures. *J. seism. Explor.*, **8**, 57–75.

Bulant, P. & Klimeš, L. (1999): Interpolation of ray-theory travel times within ray cells. *Geophys. J. int.*, **139**, 273–282. https://doi.org/10.1046/j.1365-246x.1999.00919.x

Červený, V., Klimeš, L. & Pšenčík, I. (1988): Complete seismic-ray tracing in three-dimensional structures. In: Doornbos, D.J. (ed.), *Seismological Algorithms*, Academic Press, New York, pp. 89–168.

Gajewski, D. & Pšenčík, I. (1990): Vertical seismic profile synthetics by dynamic ray tracing in laterally varying layered anisotropic structures. *J. geophys. Res.*, **95B**, 11301–11315. https://doi.org/10.1029/JB095iB07p11301

Gray, S. H., Etgen, J., Dellinger, J. & Whitmore, D. (2001): Seismic migration problems and solutions. *Geophysics*, **66**, 1622–1640. https://doi.org/10.1190/1.1487107

Hokstad, K. (2000): Multicomponent Kirchhoff migration. *Geophysics*, **65**, 861–873. https://doi.org/10.1190/1.1444783

Hou, A. & Marfurt, K. J. (2002): Multicomponent prestack depth migration by scalar wavefield extrapolation. *Geophysics*, **67**, 1886–1894. https://doi.org/10.1190/1.1527088

Klimeš, L. (2002): Relation of the wave-propagation metric tensor to the curvatures of the slowness and ray-velocity surfaces. *Stud. geophys. geod.*, **46**, 589–597. https://doi.org/10.1023/A:1019551320867

Kuo, J. T & Dai, T. (1984): Kirchhoff elastic wave migration for the case of noncoincident source and receiver. *Geophysics*, **49**, 1223–1238. https://doi.org/10.1190/1.1441751

Mensch, T. & Rasolofosaon, P. (1997): Elastic-wave velocities in anisotropic media of arbitrary symmetry-generalization of Thomsen's parameters ϵ, δ and γ. *Geophys. J. Int.*, **128**, 43–64. https://doi.org/10.1111/j.1365-246X.1997.tb04070.x

Qizhen, D. & Bo, H. (2008): Elastic Kirchhoff migration of vectorial wave-fields. *Applied Geophysics*, **5**(4), 284–293. https://doi.org/10.1007/s11770-008-0045-z

Versteeg, R. J. & Grau, G. (eds.) (1991): The Marmousi experience. *Proc. EAGE workshop on Practical Aspects of Seismic Data Inversion (Copenhagen, 1990)*, Eur. Assoc. Explor. Geophysicists, Zeist.

Wang, W. & McMechan, G. A. (2016): Vector-based image condition for 3D elastic reverse time migrations. *Expanded Abstr., 86th Ann. Internat. SEG Mtg.*, 4168–4172.